Strongly modified four-wave mixing in a coupled semiconductor quantum dot-metal nanoparticle system

Emmanuel Paspalakis, Sofia Evangelou, Spyridon G. Kosionis, and Andreas F. Terzis

Citation: Journal of Applied Physics **115**, 083106 (2014); doi: 10.1063/1.4866424
View online: http://dx.doi.org/10.1063/1.4866424
View Table of Contents: http://scitation.aip.org/content/aip/journal/jap/115/8?ver=pdfcov
Published by the AIP Publishing

Strongly modified four-wave mixing in a coupled semiconductor quantum dot-metal nanoparticle system

Emmanuel Paspalakis,[1,a)] Sofia Evangelou,[1,2] Spyridon G. Kosionis,[3] and Andreas F. Terzis[3]
[1]*Materials Science Department, School of Natural Sciences, University of Patras, 265 04 Patras, Greece*
[2]*Department of Materials Science and Engineering, University of Ioannina, Ioannina 45110, Greece*
[3]*Department of Physics, School of Natural Sciences, University of Patras, 265 04 Patras, Greece*

(Received 23 January 2014; accepted 9 February 2014; published online 26 February 2014)

We study the four-wave mixing effect in a coupled semiconductor quantum dot-spherical metal nanoparticle structure. Depending on the values of the pump field intensity and frequency, we find that there is a critical distance that changes the form of the spectrum. Above this distance, the four-wave mixing spectrum shows an ordinary three-peaked form and the effect of controlling its magnitude by changing the interparticle distance can be obtained. Below this critical distance, the four-wave mixing spectrum becomes single-peaked; and as the interparticle distance decreases, the spectrum is strongly suppressed. The behavior of the system is explained using the effective Rabi frequency that creates plasmonic metaresonances in the hybrid structure. In addition, the behavior of the effective Rabi frequency is explained via an analytical solution of the density matrix equations. © *2014 AIP Publishing LLC*. [http://dx.doi.org/10.1063/1.4866424]

I. INTRODUCTION

The study of the optical properties of complex photonic structures that involve the interaction of excitons from semiconductor quantum dots and surface plasmons from metallic nanostructures has attracted significant attention recently both theoretically[1–35] and experimentally.[36–42] This is a relatively new area of active research in nanophotonics and falls within quantum plasmonics.[43] A structure that has attracted particular attention is a hybrid nanocrystal complex composed of a semiconductor quantum dot and a spherical metal nanoparticle.[1,3–14,16–19,22–27,29–32,34]

The optical response of this structure interacting with a weak probe field of varying frequency and a strong pump field of fixed frequency has already been considered in some works.[5,7,12,19,32] In particular, Lu and Zhu[7] investigated the probe absorption and dispersion of the probe field in the presence of the pump field and showed that a hole induced by coherent population oscillation appears at the absorption spectrum of the probe field when excitons and plasmons interact. They also pointed out that the system may exhibit slow light and that the slow light effect is greatly modified by the distance between the quantum dot and the metal nanoparticle due to the coupling of excitons and plasmons. In the same system, Sadeghi[12,32] studied the generation of tunable gain without inversion in semiconductor quantum dots using plasmonic effects. He showed that when such a system is exposed to a laser field and the interparticle distance is reduced, the initial impact of plasmons is enhancement of the ac-Stark shift in the quantum dot. Moreover, when this distance reaches a critical value, a creation of plasmonic metaresonances occurs[6] and an abrupt formation of a significant amount of gain without inversion in the quantum dot appears.

Another nonlinear optical phenomenon that has been studied in the same complex nanostructure is the four-wave mixing.[5] Initially, Lu and Zhu[5] showed that significantly enhanced four-wave mixing can occur due to exciton-plasmon interaction, and that the spectrum of the real and imaginary part of the relevant $\chi^{(3)}$ susceptibility is significantly dependent on the distance between the quantum dot and the metal nanoparticle. Quite recently, Li *et al.*[19] predicted induced bistable behavior of the real and imaginary part of the $\chi^{(3)}$ susceptibility of the four-wave mixing effect. They gave specific emphasis to the behavior of the relevant $\chi^{(3)}$ susceptibility in the bistability region and showed that the bistability region can be tuned by adjusting the size of metal nanoparticle, the interparticle distance and the intensity of the pump field.

In this paper, we also address the problem of the four-wave mixing in a coupled semiconductor quantum dot-spherical metal nanoparticle structure and give emphasis to the behavior of the four-wave mixing spectrum with the interparticle distance. We find that there is a critical interparticle distance that strongly modifies the four-wave mixing spectrum. This critical distance is the one that creates plasmonic metaresonances in the hybrid structure.[6,12] Above this critical distance, the four-wave mixing spectrum shows an ordinary three-peaked form and the effect of controlling its magnitude by changing the interparticle distance can be obtained. Below this critical distance, the four-wave mixing spectrum becomes single-peaked; and as the interparticle distance decreases, the spectrum is strongly suppressed.

The paper is organized as follows: in Sec. II, we present the density matrix equations for the several nonlinear optical processes due to the interaction of the semiconductor quantum dot system with the pump and probe electromagnetic fields in the presence of the metal nanoparticle. Then, in Sec. III, we present results obtained from numerical solutions of the density matrix equations and study systematically the dependence of the four-wave mixing spectrum on

a)Electronic mail: paspalak@upatras.gr

interparticle distance, pump field intensity, and frequency. Moreover, an explanation of the behavior of the four-wave mixing spectrum is given in terms of an effective Rabi frequency. Finally, in Sec. IV, we summarize our findings.

II. THEORETICAL METHODOLOGY

The hybrid structure that we study is composed of a spherical metal nanoparticle of radius α and a small spherical semiconductor quantum dot of radius β, in an environment with real dielectric constant ε_{env}, see Fig. 1. The center-to-center distance between the two particles is denoted by R. We also assume that $\beta \ll \alpha$ and consider that $R > \alpha$. The quantum dot is characterized by a two-level system, with $|1\rangle$ being the ground state and $|2\rangle$ being the single exciton state. The biexciton state is omitted here. This is an approximation that has been done in all the theoretical papers in this area.[1–32] For CdSe-based quantum dots, that are of interest here, the biexciton binding energy is large (for example, values up to 50 meV have been reported by Sewall *et al.*[44]) and its value increases as the quantum dot size decreases.[44] Therefore, we do not expect the biexciton state to have significant influence in the system studied here. The energy difference between the two states is $\hbar\omega_0$. This system interacts with two linearly polarized oscillating electromagnetic fields, a pump, and a probe field, with total electric field

$$\vec{E}(t) = \hat{z}[E_a \cos(\omega_a t) + E_b \cos(\omega_b t)] \tag{1}$$

that excites the interband transition between the two energy levels of the semiconductor quantum dot. Here, $\hat{z}$ is the polarization unit vector (along the z direction), E_a (E_b) is the electric field amplitude of the pump (probe) field, and ω_a (ω_b) is the angular frequency of the pump (probe) applied field. The dielectric constant of the semiconductor quantum dot is represented by ε_S, while we treat the metal nanoparticle as a classical dielectric particle with dielectric function $\varepsilon_m(\omega)$.

The electromagnetic field also excites plasmons, on the surface of the metal nanoparticle. These plasmonic excitations provide a strong continuous spectral response. Such surface plasmons influence the excitons and induce electromagnetic interactions between excitons and plasmons.[1–3] The Hamiltonian of the system, in the dipole approximation, takes the form

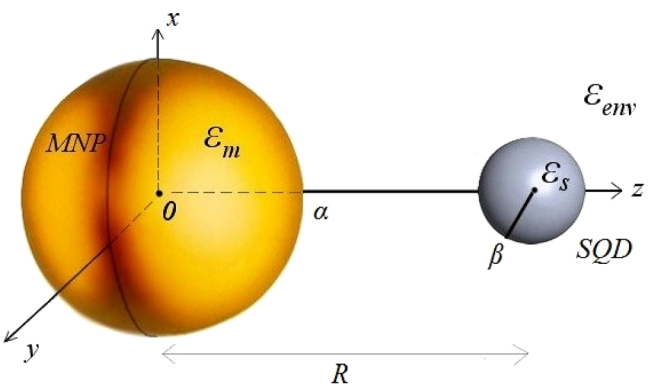

FIG. 1. The coupled system consists of a semiconductor quantum dot of radius β and a spherical metallic nanoparticle of radius α. The centers of the two particles are separated by distance R.

$$H = \hbar\omega_0|2\rangle\langle 2| - \mu E_{SQD}(t)(|1\rangle\langle 2| + |2\rangle\langle 1|), \tag{2}$$

where μ represents the dipole moment of the semiconductor quantum dot corresponding to the single exciton transition, and E_{SQD} represents the electric field inside the semiconductor quantum dot. In the dipole approximation, the total electric field inside the quantum dot consists of two parts, the first part being the applied external fields and the second part corresponding to the induced fields produced by the polarization of the metal nanoparticle (treated as a classical metallic nanosphere). E_{SQD}, in the quasi-static approximation, is explicitly written as[1,3,14]

$$E_{SQD}(t) = \frac{\hbar}{\mu}\sum_{n=a,b}\left[\frac{\Omega_n}{2}e^{-i\omega_n t} + G_n\rho_{21}(t) + \frac{\Omega_n^*}{2}e^{i\omega_n t} + G_n^*\rho_{12}(t)\right] \tag{3}$$

with $\rho_{nm}(t)$ being the density matrix elements. We also defined the Rabi frequencies of the pump (Ω_a) and probe (Ω_b) fields as[1,3,14]

$$\Omega_n = \frac{\mu E_n}{\hbar\varepsilon_{effS}}\left(1 + \frac{s_a\gamma_n\alpha^3}{R^3}\right), \tag{4}$$

and the parameter G_n as[1,14]

$$G_n = \frac{1}{4\pi\varepsilon_{env}}\frac{s_a^2\gamma_n\alpha^3\mu^2}{\hbar\varepsilon_{effS}^2 R^6}. \tag{5}$$

Here, $\varepsilon_{effS} = \frac{2\varepsilon_{env}+\varepsilon_S}{3\varepsilon_{env}}$, $\gamma_n = \frac{\varepsilon_m(\omega_n)-\varepsilon_{env}}{\varepsilon_m(\omega_n)+2\varepsilon_{env}}$ with $n = a,\ b$, and $s_a = 2$ as the applied field is taken parallel to the interparticle axis of the system (the interparticle axis is the z-axis). The Rabi frequency has two terms, the first related to the direct coupling of the quantum dot to the applied field and the second term related to the electric field from the metal nanoparticle that is induced by the external applied field. In other words, the external applied field induces a dipole moment on the metal nanoparticle, which then acts as a single dipole producing the dipolar interaction with the quantum dot showing the well-known $1/R^3$ dependence with the distance between the two particles. In addition, the parameter G_n arises due to the dipole-dipole interactions between excitons and plasmons. This term originates from the induced dipole on the metal nanoparticle, which is now produced by the dipole induced by the applied field on the semiconductor quantum dot.[1,14] G_n is also called the self-interaction term of the quantum dot[14] and is responsible for the Förster energy transfer between the quantum dot and the metal nanoparticle.[18]

We introduce the slowly varying quantities of the density matrix elements $\sigma_{21}(t) = \rho_{21}(t)e^{i\omega_a t}$, $\sigma_{12}(t) = \rho_{12}(t)e^{-i\omega_a t}$, $\sigma_{11}(t) = \rho_{11}(t)$, $\sigma_{22}(t) = \rho_{22}(t)$ and obtain the density matrix equations, which describe the dynamics of the system, under the rotating wave approximation as

$$\dot{\sigma}_{21}(t) = -\left(i\Delta_a + \frac{1}{T_2}\right)\sigma_{21}(t) - iG[\sigma_{22}(t) - \sigma_{11}(t)]\sigma_{21}(t) - \frac{i}{2}\left(\Omega_a + \Omega_b e^{-i\delta t}\right)[\sigma_{22}(t) - \sigma_{11}(t)], \tag{6}$$

$$\dot{\sigma}_{22}(t)-\dot{\sigma}_{11}(t)=i\left(\Omega_a+\Omega_b e^{-i\delta t}\right)\sigma_{12}(t) -i(\Omega_a^*+\Omega_b^* e^{i\delta t})\sigma_{21}(t)-4G_I\sigma_{21}(t)\sigma_{12}(t) -\frac{\sigma_{22}(t)-\sigma_{11}(t)+1}{T_1}. \quad (7)$$

In Eqs. (6) and (7), $\Delta_a=\omega_0-\omega_a$ is the detuning of the pump field from resonance, $\delta=\omega_b-\omega_a$ is the detuning between the two fields, and G_I represents the imaginary part of the parameter $G=G_a+G_b$. Moreover, T_1 is the population relaxation time due to spontaneous emission and T_2 is the relaxation due to dephasing processes of the semiconductor quantum dot. The relaxation times T_1 and T_2 are in principle influenced by the presence of the metal nanoparticle; however for the parameters that we use here, the values of T_1 and T_2 do not practically change in the frequency region of interest, and therefore will be considered constant in this study, as in previous papers concerning similar systems.[1–21,23–32]

We take that the pump field is a strong field and its interaction with the system will be treated to all orders while the probe field is a weak field and its interaction with the system will be treated to first order. This means that $|\Omega_b|\ll|\Omega_a|$. We then expand $\sigma_{21}(t)$ as[45–47]

$$\sigma_{21}(t)=\sigma_{21}^{(\omega_a)}(t)+\sigma_{21}^{(\omega_b)}(t)e^{-i\delta t}+\sigma_{21}^{(2\omega_a-\omega_b)}(t)e^{i\delta t}, \quad (8)$$

and $\sigma_{22}(t)-\sigma_{11}(t)$ as[45–47]

$$\sigma_{22}(t)-\sigma_{11}(t)=w^{(0)}(t)+w^{(-\delta)}(t)e^{i\delta t}+w^{(\delta)}(t)e^{-i\delta t}. \quad (9)$$

Here, $w^{(0)}(t)$ is the population inversion and $\sigma_{21}^{(\omega_a)}(t)$ is the off-diagonal term of the matrix element in the case that $E_b=0$. Also, $w^{(\delta)}(t)=w^{(-\delta)^*}(t)$ as the population difference should be real. The last two terms describe the effect of population pulsation in the system.[45] The terms $\sigma_{21}^{(\omega_b)}(t)$, $\sigma_{21}^{(2\omega_a-\omega_b)}(t)$, $w^{(-\delta)}(t)$, $w^{(\delta)}(t)$ are considered to be small, in the sense that $|\sigma_{21}^{(\omega_b)}(t)|$, $|\sigma_{21}^{(2\omega_a-\omega_b)}(t)|\ll|\sigma_{21}^{(\omega_a)}(t)|$ and $|w^{(-\delta)}(t)|$, $|w^{(\delta)}(t)|\ll|w^{(0)}(t)|$. We also define $\sigma_{12}^{(-\omega_a)}(t)=\sigma_{21}^{(\omega_a)^*}(t)$, $\sigma_{12}^{(-\omega_b)}(t)=\sigma_{21}^{(\omega_b)^*}(t)$, and $\sigma_{12}^{(\omega_b-2\omega_a)}(t)=\sigma_{21}^{(2\omega_a-\omega_b)^*}(t)$.

Following the above procedure, we obtain the following differential equations for the density matrix elements:

$$\dot{w}^{(0)}(t)=i\left[\Omega_a\sigma_{12}^{(-\omega_a)}(t)-\Omega_a^*\sigma_{21}^{(\omega_a)}(t)\right] -4G_I\sigma_{12}^{(-\omega_a)}(t)\sigma_{21}^{(\omega_a)}(t)-\frac{w^{(0)}(t)+1}{T_1}, \quad (10)$$

$$\dot{w}^{(-\delta)}(t)=-\left(i\delta+\frac{1}{T_1}\right)w^{(-\delta)}(t)+i\Omega_a\sigma_{12}^{(-\omega_b)}(t) -i\Omega_a^*\sigma_{21}^{(2\omega_a-\omega_b)}(t)-i\Omega_b^*\sigma_{21}^{(\omega_a)}(t) -4G_I\left[\sigma_{12}^{(-\omega_b)}(t)\sigma_{21}^{(\omega_a)}(t)+\sigma_{12}^{(-\omega_a)}(t)\sigma_{21}^{(2\omega_a-\omega_b)}(t)\right], \quad (11)$$

$$\dot{\sigma}_{21}^{(\omega_a)}(t)=-\left(i\Delta_a+\frac{1}{T_2}\right)\sigma_{21}^{(\omega_a)}(t)-i\frac{\Omega_a}{2}w^{(0)}(t) -iG\sigma_{21}^{(\omega_a)}(t)w^{(0)}(t), \quad (12)$$

$$\dot{\sigma}_{21}^{(\omega_b)}(t)=-\left(i\Delta_a-i\delta+\frac{1}{T_2}\right)\sigma_{21}^{(\omega_b)}(t)-i\frac{\Omega_a}{2}w^{(\delta)}(t) -iG\sigma_{21}^{(\omega_a)}(t)w^{(\delta)}(t) -iG\sigma_{21}^{(\omega_b)}(t)w^{(0)}(t)-i\frac{\Omega_b}{2}w^{(0)}(t), \quad (13)$$

$$\dot{\sigma}_{21}^{(2\omega_a-\omega_b)}(t)=-\left(i\Delta_a+i\delta+\frac{1}{T_2}\right)\sigma_{21}^{(2\omega_a-\omega_b)}(t)-i\frac{\Omega_a}{2}w^{(-\delta)}(t) -iG\sigma_{21}^{(\omega_a)}(t)w^{(-\delta)}(t)-iG\sigma_{21}^{(2\omega_a-\omega_b)}(t)w^{(0)}(t). \quad (14)$$

We will solve these equations for the description of the four-wave mixing process. The essential difference of Eqs. (10)–(14) and those describing two-level systems without the plasmonic nanostructure[45–47] is due to the nonlinear terms, i.e., the terms containing the parameter G. As Eqs. (10)–(14) are nonlinear differential equations, we will follow a numerical solution of them using a Runge-Kutta method. The four-wave mixing spectrum is given by[45–48]

$$FWM=|\sigma_{21}^{(2\omega_a-\omega_b)}(t=T)|^2, \quad (15)$$

where T is the time length of the applied electromagnetic fields that is taken long enough so as the system under study has reached steady state behavior.

Equations (10) and (12) can be solved independently. Combining the steady state solutions of these two equations, we find that the steady state population inversion can be calculated as one of the roots of a third-order equation[22]

$$w_{ss}^{(0)3}+c_2w_{ss}^{(0)2}+c_1w_{ss}^{(0)}+c_0=0, \quad (16)$$

where

$$c_2=1+\frac{2T_2^2\Delta_aG_R-2T_2G_I}{T_2^2|G|^2}, \quad (17)$$

$$c_1=\frac{T_1T_2|\Omega_a|^2+T_2^2\Delta_a^2+2T_2^2\Delta_aG_R-2T_2G_I+1}{T_2^2|G|^2}, \quad (18)$$

$$c_0=\frac{1+T_2^2\Delta_a^2}{T_2^2|G|^2}, \quad (19)$$

with $w_{ss}^{(0)}$ denoting the value of $w^{(0)}(t)$ in steady state and G_R being the real part of the parameter G.

The solutions for $w_{ss}^{(0)}$ are

$$(w_{ss}^{(0)})_1=p_++p_--\frac{c_2}{3}, \quad (20)$$

$$(w_{ss}^{(0)})_2=-\frac{p_++p_-}{2}-\frac{c_2}{3}+i\frac{\sqrt{3}}{2}(p_+-p_-), \quad (21)$$

$$(w_{ss}^{(0)})_3=-\frac{p_++p_-}{2}-\frac{c_2}{3}-i\frac{\sqrt{3}}{2}(p_+-p_-), \quad (22)$$

where

$$p_\pm=\left(r\pm\sqrt{S}\right)^{1/3}, \quad (23)$$

$$q = \frac{3c_1 - c_2^2}{9}, \tag{24}$$

$$r = \frac{9c_1c_2 - 27c_0 - 2c_2^3}{54}, \tag{25}$$

$$S = q^3 + r^2. \tag{26}$$

As $w_{ss}^{(0)}$ represents the population inversion, we only account for the real roots that satisfy the condition $-1 \leq w_{ss}^{(0)} \leq 1$. These solutions will be used in the Sec. III for the explanation of the behavior of the four-wave mixing spectrum.

III. NUMERICAL RESULTS

In all the calculations, we take the quantum dot initially in the ground state, leading to $w^{(0)}(0) = -1$ and the rest density matrix elements being zero. The parameters that we use are $T_1 = 0.8$ ns, $T_2 = 0.3$ ns, $\varepsilon_{env} = \varepsilon_0$, $\alpha = 7.5$ nm, $\mu = 0.65\,e$ nm, $\hbar\omega_0 = 2.5$ eV, $\varepsilon_S = 6\varepsilon_0$, with ε_0 being the dielectric constant of the vacuum. These values correspond to colloidal quantum dots (typically CdSe-based quantum dots) and have been used in various studies.[1,3,6,9,14,16,18,22,24,29] For $\varepsilon_m(\omega)$, we use experimental values of gold.[49] We solve numerically, using a fourth-order Runge-Kutta method, Eqs. (10)–(14) for $T = 100$ ns to obtain the steady state behavior of the spectrum. Below, in all calculations, the intensity of the probe field is taken four orders of magnitude smaller than the intensity of the pump field.

In Fig. 2, we present the four-wave mixing spectrum for different interparticle distances when the pump field is at exact resonance with the quantum dot, $\Delta_a = 0$. Results for two different pump field intensities are shown. From Figs. 2(a) and 2(b), we find that for both pump field intensities, the spectrum is triple peaked, with one peak at $\delta = 0$ and two symmetric peaks at positive and negative values of δ. These are called Rabi sidebands. The decrease of the interparticle distance increases the magnitude of the four-wave mixing spectrum. In addition, the positions of the Rabi sidebands change to larger or smaller detunings depending on the interparticle distance and the pump field intensity. These results are in agreement with that of Refs. 5 and 19, where the real and imaginary part of the susceptibility, which are responsible for the four-wave mixing process were presented. However, for even smaller interparticle distances, the results are markedly different, as can be seen in Figs. 2(c) and 2(d). There, the spectrum is single-peaked and as the interparticle distance decreases the spectrum is suppressed. The same general behavior is found in Figs. 3 and 4 that the pump field is detuned from resonance, for both positive (Fig. 3) and negative (Fig. 4) detunings. We note that the form of the spectrum and the actual distance for which the form of the spectrum changes from triple-peaked to single-peaked depends on the pump field intensity and frequency; and for a certain value of the distance, the spectrum can be either triple-peaked or single-peaked depending on the values of the pump field intensity and frequency. For the dependence on pump intensity, see, for example, the case of $R = 15$ nm in Figs. 2(b) and 2(c).

The explanation of the form of the four-wave mixing spectrum shown in Figs. 2 to 4 lies in the behavior of the effective Rabi frequency

$$\Omega_{\text{eff}} = \Omega_a + 2G\sigma_{21}^{(\omega_a)ss}, \tag{27}$$

where $\sigma_{21}^{(\omega_a)ss}$ denotes the value of $\sigma_{21}^{(\omega_a)}(t)$ in steady state.[6,12] The effective Rabi frequency Ω_{eff} is defined in order to make the nonlinear density matrix Eqs. (10)–(14) in steady state to be written in the same form as the (linear) density matrix equations of a regular two-level system,[46] where the pump field Rabi frequency has been replaced by the effective Rabi frequency. Of course, the effective Rabi frequency is not a regular Rabi frequency as its value depends on the value of the density matrix element $\sigma_{21}^{(\omega_a)ss}$; however, it can be used

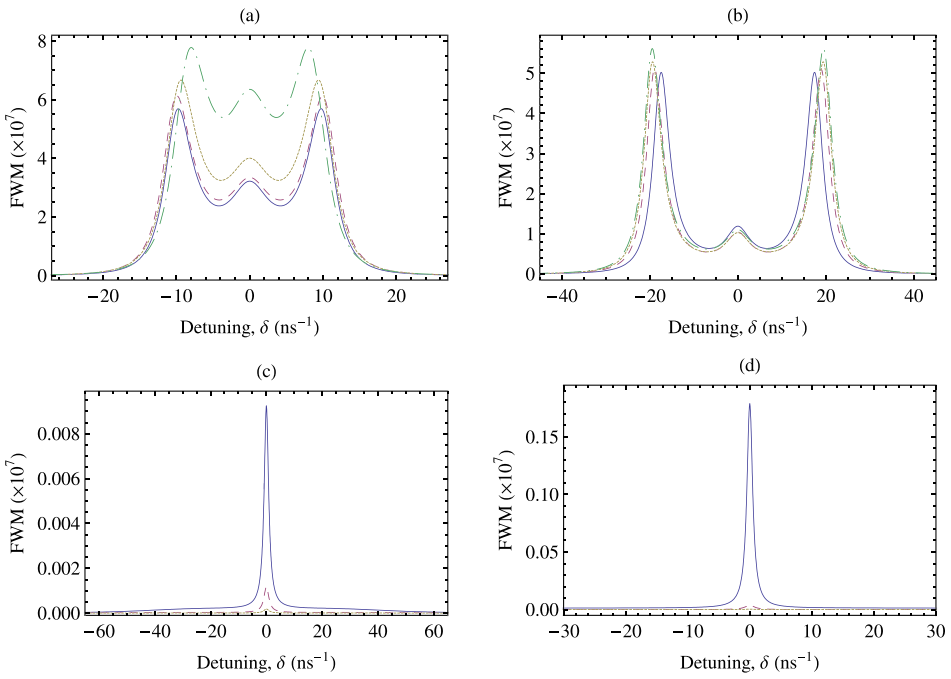

FIG. 2. The four-wave mixing spectra in the coupled system as a function of the detuning δ. The intensity of the pump field is $I_a = 10^2$ W/cm^2 in (a) and (c) and $I_a = 3 \times 10^2$ W/cm^2 in (b) and (d). The pump field excitation is at exact resonance, $\Delta_a = 0$. In (a), solid curve $R = 100$ nm, dashed curve $R = 20$ nm, dotted curve $R = 18$ nm, and dotted-dashed curve $R = 16.5$ nm. In (b), solid curve $R = 100$ nm, dashed curve $R = 20$ nm, dotted curve $R = 17$ nm, and dotted-dashed curve $R = 15$ nm. In (c), solid curve $R = 15$ nm, dashed curve $R = 14.5$ nm, and dotted curve $R = 14$ nm. In (d), solid curve $R = 14$ nm, dashed curve $R = 13.5$ nm, and dotted curve $R = 13$ nm.

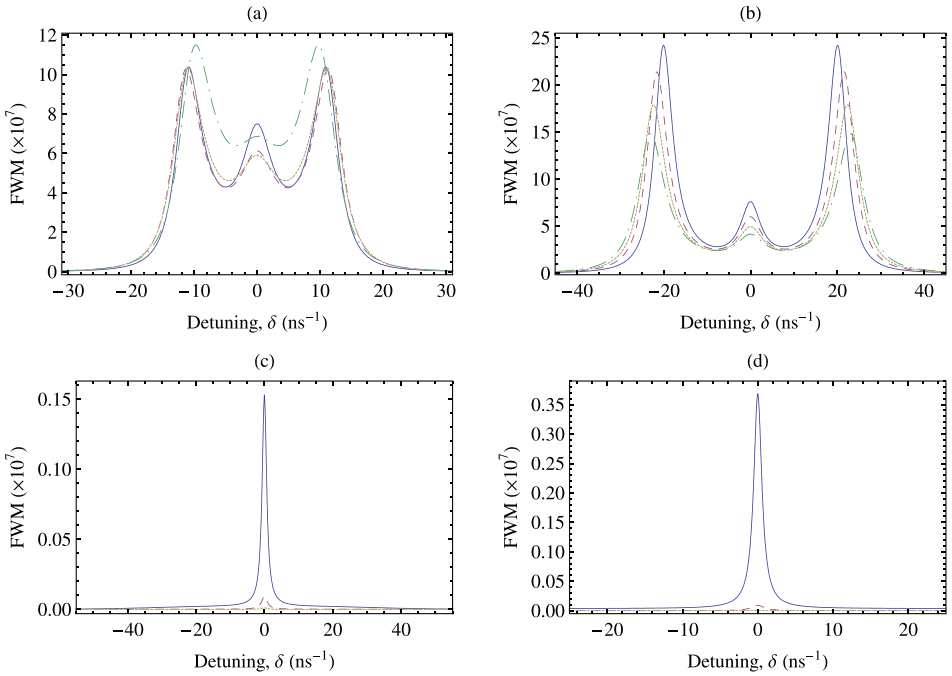

FIG. 3. The four-wave mixing spectra in the coupled system as a function of the detuning δ. The intensity of the pump field is $I_a = 10^2\,\mathrm{W/cm^2}$ in (a) and (c) and $I_a = 3\times10^2\,\mathrm{W/cm^2}$ in (b) and (d). The pump field excitation is detuned by $\Delta_a = 5\,\mathrm{ns^{-1}}$ in (a) and (c) and $\Delta_a = 10\,\mathrm{ns^{-1}}$ in (b) and (d). In (a) solid curve $R = 100\,\mathrm{nm}$, dashed curve $R = 20\,\mathrm{nm}$, dotted curve $R = 18\,\mathrm{nm}$, and dotted-dashed curve $R = 16\,\mathrm{nm}$. In (b) solid curve $R = 100\,\mathrm{nm}$, dashed curve $R = 20\,\mathrm{nm}$, dotted curve $R = 17\,\mathrm{nm}$, and dotted-dashed curve $R = 15\,\mathrm{nm}$. In (c) solid curve $R = 15\,\mathrm{nm}$, dashed curve $R = 14.5\,\mathrm{nm}$, and dotted curve $R = 14\,\mathrm{nm}$. In (d) solid curve $R = 13.5\,\mathrm{nm}$, dashed curve $R = 13\,\mathrm{nm}$, and dotted curve $R = 12.5\,\mathrm{nm}$.

for understanding the behavior shown in Figs. 2 to 4, as can be seen from Figs. 5 and 6. From there, we note that the value of the effective Rabi frequency changes strongly with interparticle distance. This change denotes two regions, the region of large value of Ω_{eff} where the triple-peaked spectrum appears and the region of low value of Ω_{eff} where the single-peaked spectrum appears. This is an indication of plasmonic metaresonances in the system, a concept proposed and explored by Sadeghi.[6,12,32,33] These metaresonances are molecular-like resonances resulting by the conjugation of the quantum dot excitonic and the metal nanoparticle plasmonic excitations. It has been revealed by Sadeghi that these metaresonances can be associated with two distinct metastates of the quantum dot-metal nanoparticle system. The B(right) state where after an initial delay the effective electric field of the quantum dot can be quite significant resulting in an emitting quantum dot and the D(ark) state where the field experienced by the quantum dot is screened significantly at all times.[32,33] Actually, the same author defines the normalized Rabi frequency, which coincides with our effective Rabi frequency defined in Eq. (27). These two characteristic states are practically distinguished by means of the two well-separated regions found in the plots of the real and imaginary part of the normalized Rabi frequency (compare, for example, Fig. 4 in Ref. 12 and Figs. 5 and 6 in our article).

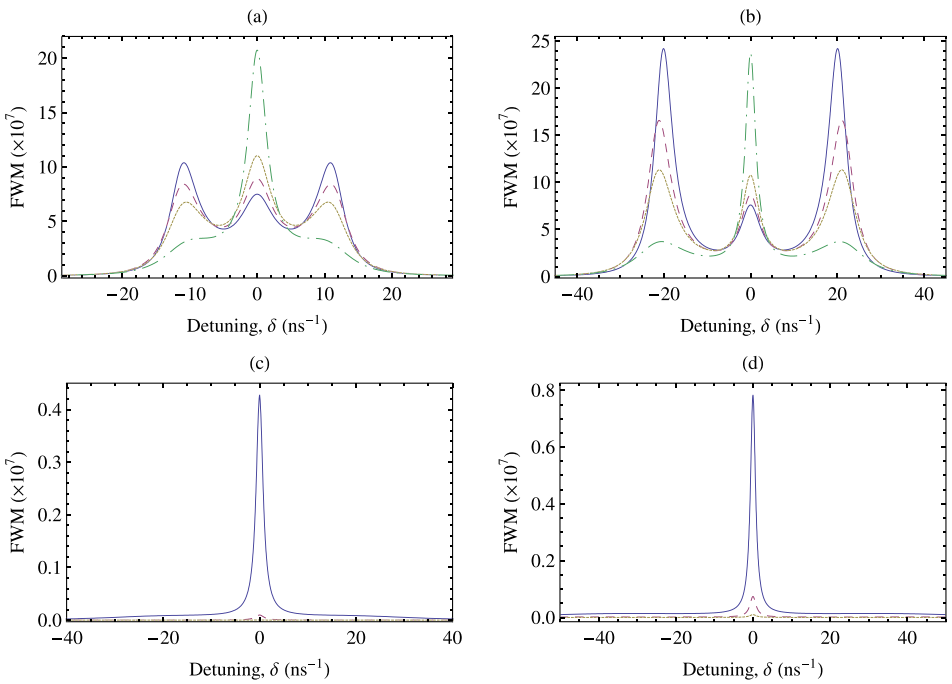

FIG. 4. The four-wave mixing spectra in the coupled system as a function of the detuning δ. The intensity of the pump field is $I_a = 10^2\,\mathrm{W/cm^2}$ in (a) and (c) and $I_a = 3\times10^2\,\mathrm{W/cm^2}$ in (b) and (d). The pump field excitation is detuned by $\Delta_a = -5\,\mathrm{ns^{-1}}$ in (a) and (c) and $\Delta_a = -10\,\mathrm{ns^{-1}}$ in (b) and (d). In (a) solid curve $R = 100\,\mathrm{nm}$, dashed curve $R = 22\,\mathrm{nm}$, dotted curve $R = 20\,\mathrm{nm}$, and dotted-dashed curve $R = 18\,\mathrm{nm}$. In (b) solid curve $R = 100\,\mathrm{nm}$, dashed curve $R = 20\,\mathrm{nm}$, dotted curve $R = 18\,\mathrm{nm}$, and dotted-dashed curve $R = 16\,\mathrm{nm}$. In (c) solid curve $R = 16\,\mathrm{nm}$, dashed curve $R = 15\,\mathrm{nm}$, and dotted curve $R = 14\,\mathrm{nm}$. In (d) solid curve $R = 14.5\,\mathrm{nm}$, dashed curve $R = 14\,\mathrm{nm}$, and dotted curve $R = 13.5\,\mathrm{nm}$.

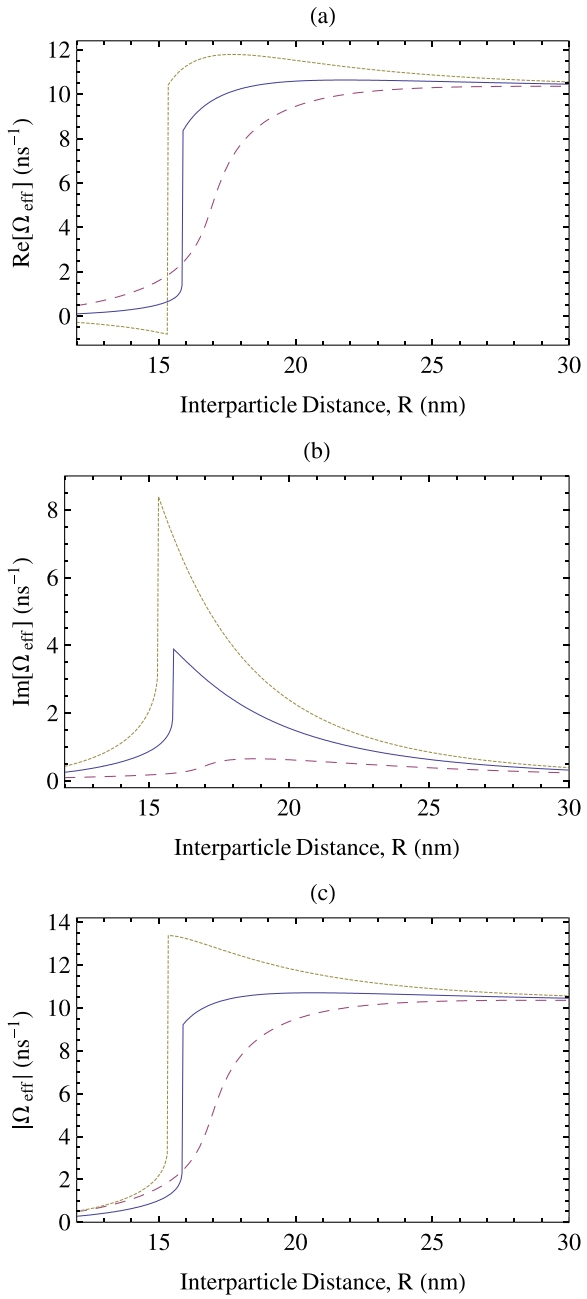

FIG. 5. The real (a), imaginary (b), and absolute value (c) of the effective Rabi frequency Ω_{eff} as a function of the interparticle distance R. The intensity of the pump field is $I_a = 10^2\,\text{W/cm}^2$ and the pump field detuning is $\Delta_a = 0$ (solid curve), $\Delta_a = -5\,\text{ns}^{-1}$ (dashed curve), and $\Delta_a = 5\,\text{ns}^{-1}$ (dotted curve).

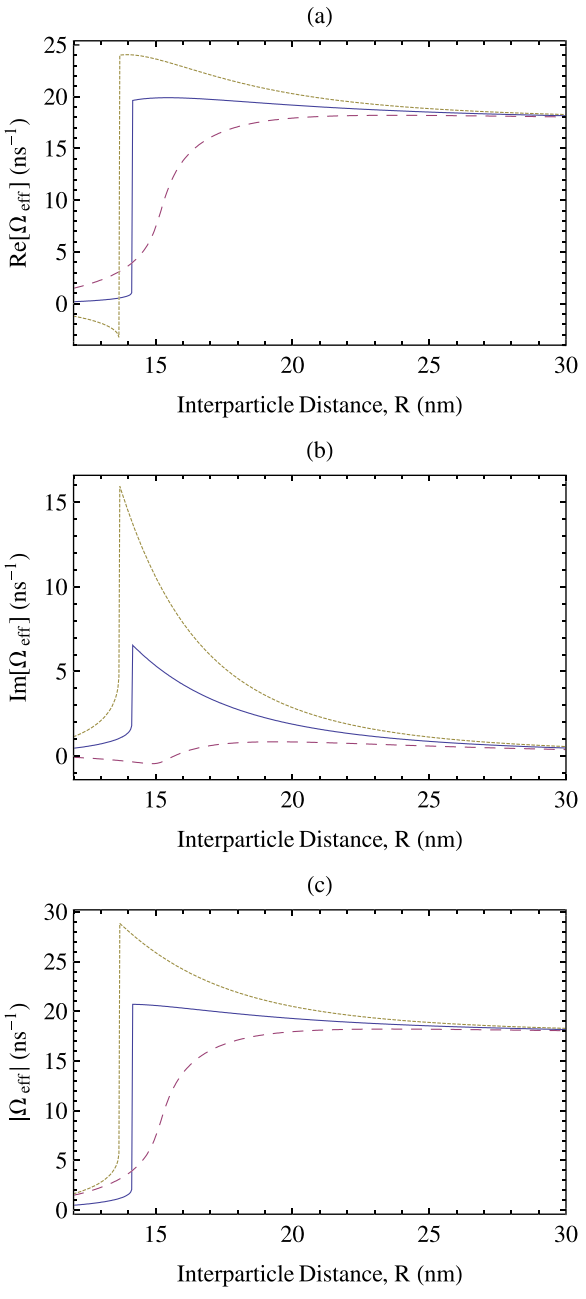

FIG. 6. The real (a), imaginary (b), and absolute value (c) of the effective Rabi frequency Ω_{eff} as a function of the interparticle distance R. The intensity of the pump field is $I_a = 3 \times 10^2\,\text{W/cm}^2$ and the pump field detuning is $\Delta_a = 0$ (solid curve), $\Delta_a = -10\,\text{ns}^{-1}$ (dashed curve), and $\Delta_a = 10\,\text{ns}^{-1}$ (dotted curve).

We also find that the positions of the Rabi sidebands are roughly approximated by $\delta = \pm\sqrt{\Delta_a^2 + |\Omega_{\text{eff}}|^2}$. The larger values of $|\Omega_{\text{eff}}|$ are obtained for positive detunings of the pump field and the lower values for negative detunings of the pump field. Also, for negative detunings of the pump field, the change between the two regions of Ω_{eff} is rather smooth; while for zero or positive detunings, this change is rather abrupt.

The behavior of Ω_{eff} can be used for determining the critical distance that changes the form of the spectrum from triple-peaked to single-peaked as the distance decreases. For the case of zero or positive detunings, the critical distance is the distance that the abrupt change in the value of Ω_{eff} occurs. For example, for the case of Fig. 5, these values are approximately 15.855 nm for $\Delta_a = 0$ and 15.335 nm for $\Delta_a = 5\,\text{ns}^{-1}$. For the case of negative detunings, the exact value of the critical distance is not uniquely defined as the change in Ω_{eff} occurs smoothly, however a region of distances that this change occurs can still be determined. For example, for the case of Fig. 5, these values are approximately in the region 16.5 nm to 17.5 nm.

In order to further stress that the pump field detuning can be used for the control of the form of the four-wave mixing spectrum, we present in Fig. 7 the spectrum for the same

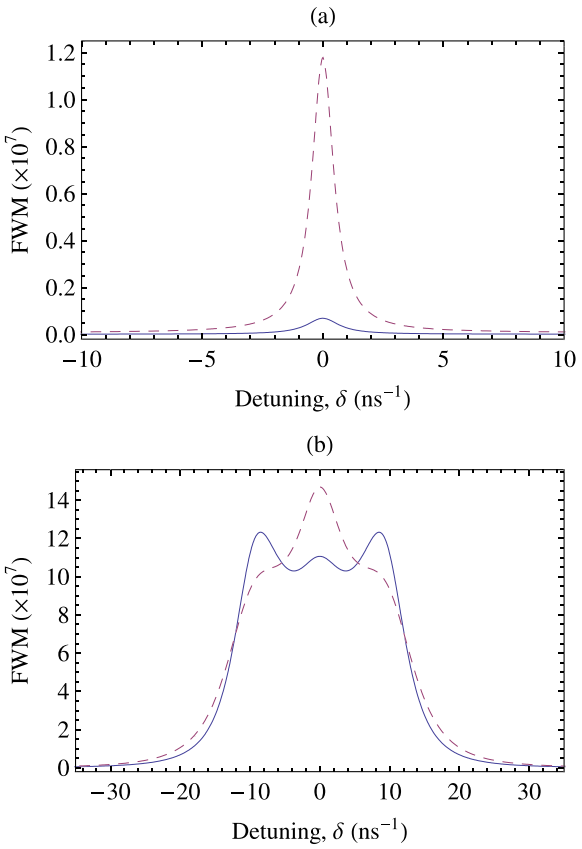

FIG. 7. The four-wave mixing spectra in the coupled system as a function of the detuning δ. The intensity of the pump field is $I_a = 10^2\,\mathrm{W/cm^2}$ and the pump field detuning is $\Delta_a = 1\,\mathrm{ns}^{-1}$ in (a) solid curve, $\Delta_a = 4\,\mathrm{ns}^{-1}$ in (a) dashed curve, $\Delta_a = 7\,\mathrm{ns}^{-1}$ in (b) solid curve, and $\Delta_a = 10\,\mathrm{ns}^{-1}$ in (b) dashed curve. The interparticle distance is $R = 15.3\,\mathrm{nm}$ in every case.

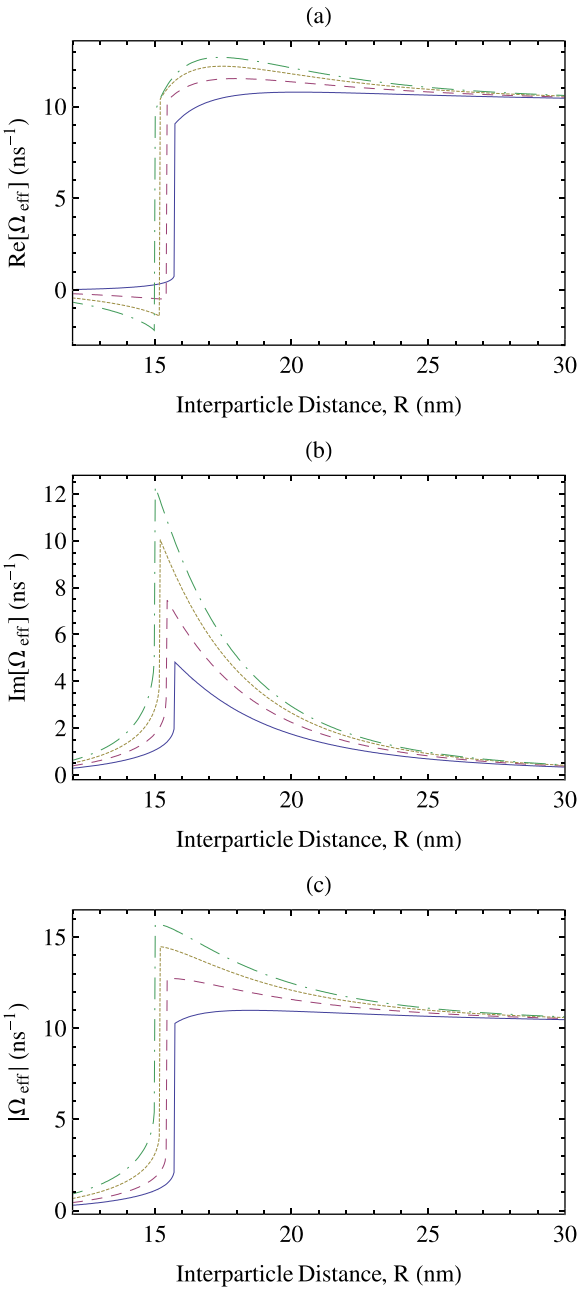

FIG. 8. The real (a), imaginary (b), and absolute value (c) of the effective Rabi frequency Ω_{eff} as a function of the interparticle distance R. The intensity of the pump field is $I_a = 10^2\,\mathrm{W/cm^2}$ and the pump field detuning is $\Delta_a = 1\,\mathrm{ns}^{-1}$ (solid curve), $\Delta_a = 4\,\mathrm{ns}^{-1}$ (dashed curve), $\Delta_a = 7\,\mathrm{ns}^{-1}$ (dotted curve), and $\Delta_a = 10\,\mathrm{ns}^{-1}$ (dashed-dotted curve).

interparticle distance and pump field intensity, but for different values of the pump field detuning. This shows that the spectrum changes from single-peaked in Fig. 7(a) to triple-peaked in Fig. 7(b). The explanation of this is shown in Fig. 8, where it can be seen that the value of Ω_{eff} changes from the region of low value to the region of large value with the increase of the detuning of the pump field for the specific value of interparticle distance.

For the explanation of the behavior of Ω_{eff}, the relation between Ω_{eff} and $w_{ss}^{(0)}$ will be used. From Eqs. (10) and (12), with the use of Eq. (27), we obtain

$$|\Omega_{\mathrm{eff}}|^2 = -\frac{1+T_2^2\Delta_a^2}{T_1T_2}\left(1+\frac{1}{w_{ss}^{(0)}}\right). \tag{28}$$

The solutions of the third-order equation describing $w_{ss}^{(0)}$, Eqs. (20)–(22) strongly depend on the values of the parameters of the system, as can be seen by the expressions for the coefficients of the third-order algebraic equation, Eqs. (17)–(19). The nature of the roots is purely determined by the parameter S. We have one real root and two complex roots, with $(w_{ss}^{(0)})_2 = (w_{ss}^{(0)})_3^*$, when $S \geq 0$ and three real roots (bistability case[16,19,30]) when $S < 0$.

We start with the $\Delta_a = 0$ case, and try to explain the observed behavior of the magnitude of Ω_{eff} [solid curve in Fig. 5(c)] by understanding the behavior of $w_{ss}^{(0)}$. We find that for short distances between the quantum dot and the metal nanoparticle, the parameter S is positive and we have just one real and negative root, of rather large absolute value, for example at $R = 13\,\mathrm{nm}$, $w_{ss}^{(0)}$ is -0.96. As the interparticle distance increases, the absolute value of the population inversion decreases, and at $R = 14.5\,\mathrm{nm}$ and $R = 15.25\,\mathrm{nm}$ $w_{ss}^{(0)}$ becomes -0.87 and -0.75, respectively. At $R = 15.305\,\mathrm{nm}$, the parameter S becomes zero; and then for a just higher value of the interparticle distance, it becomes negative and we obtain three real roots (-0.74, -0.09, and -0.08) for $w_{ss}^{(0)}$. In the region from $R = 15.305\,\mathrm{nm}$ to $R = 15.8547\,\mathrm{nm}$, the S-parameter is always negative and the

three real roots are all negative. The largest one, $(w_{ss}^{(0)})_1$, decreases in absolute value as the distance increases. Also, the second root, $(w_{ss}^{(0)})_2$, increases in absolute value with the increase of the interparticle distance. In addition, the third root, $(w_{ss}^{(0)})_3$, has a rather small value and a weak *R*–dependence, as at the two limits of the bistability region, i.e., at $R = 15.305$ nm and at 15.8547 nm, the root is approximately -0.08 and -0.05, respectively. At distance $R = 15.8547$ nm, the parameter *S* becomes zero. In this case, we have one root of small value (approximately -0.05) and two equal roots $(w_{ss}^{(0)})_2 = (w_{ss}^{(0)})_3$, as $p_+ = p_-$. At an interparticle distance just above 15.8547 nm, the *S*-parameter becomes positive again, and there is one real root, $(w_{ss}^{(0)})_1$, and two complex roots. At this distance, we have a very abrupt change in $w_{ss}^{(0)}$ as the two larger in absolute value real roots (for $R = 15.8547$ nm, the roots are -0.42, -0.42, and -0.05) become complex (having a rather small imaginary part) and the third one (now the only real one) has a very small value.

A very similar behavior is found for positive detuning of the pump field. For the $\Delta_a = 5\,\text{ns}^{-1}$, the bistability region in which the parameter *S* is negative is [14.32 nm – 15.3351 nm]. Hence, the largest distance at which the *S*-parameter becomes zero is 15.3351 nm; and as in the previous case at this distance, we have the occurrence of the abrupt change of the population inversion. Obviously, this is the distance at which we have the abrupt change of the magnitude of the effective Rabi frequency in the dotted curve of Fig. 5(c).

For the case of negative detuning of the pump field studied in Fig. 5(c), there are no distances for which the *S*-parameter becomes zero and therefore there is not an abrupt change in the population inversion. However, we should mention that this is not a general trend for $\Delta_a < 0$, as for small values of negative Δ_a, for example for $\Delta_a = -1\,\text{ns}^{-1}$, we have found a bistability region and an abrupt change of Ω_{eff} at a distance of 16.01 nm (not shown here).

Therefore, we conclude that the most important parameter in the explanation of the abrupt change in the magnitude of Ω_{eff} is the *S*-parameter and especially the largest distance at which it becomes zero. Applying this condition for the largest intensity of the pump field ($I_a = 3 \times 10^2\,\text{W/cm}^2$), we find $R = 14.15$ nm for $\Delta_a = 0$ and $R = 13.65$ nm for $\Delta_a = 10\,\text{ns}^{-1}$. These values are in excellent agreement with the values suggested in Fig. 6(c).

We believe that it is possible someone to derive explanations for our findings in terms of the molecular-like resonances of Sadeghi,[6,12,32,33] where the two characteristic metastates (B and D) have a strong distance (R-) and intensity (I-) dependence.[33] This is expected as these two pictures (i.e., ours in terms of the S-parameter and Sadeghi's in terms of B- and D-states) are based practically on the same physical quantity, the effective Rabi frequency defined in Eq. (27).

IV. SUMMARY

In summary, here we have studied the four-wave mixing effect in a coupled semiconductor quantum dot-spherical metal nanoparticle structure giving emphasis to the behavior of the four-wave mixing spectrum with the interparticle distance. Depending on the values of the pump field intensity and frequency, we find that there is a critical distance that changes the form of the spectrum. Above this distance, the four-wave mixing spectrum shows an ordinary three-peaked form and the effect of controlling its magnitude by changing the interparticle distance can be obtained. Below this critical distance, the four-wave mixing spectrum becomes single-peaked; and as the interparticle distance decreases, the spectrum is strongly suppressed. The behavior of the system is explained by the effective Rabi frequency that creates plasmonic metaresonances in the hybrid structure. In addition, the behavior of the effective Rabi frequency is explained via an analytical solution of the density matrix equations.

ACKNOWLEDGMENTS

This research has been co-financed by the European Union (European Social Fund—ESF) and Greek national funds through the Operational Program "Education and Lifelong Learning" of the National Strategic Reference Framework (NSRF)—Research Funding Program: Heracleitus II. Investing in knowledge society through the European Social Fund.

[1]W. Zhang, A. O. Govorov, and G. W. Bryant, Phys. Rev. Lett. **97**, 146804 (2006).
[2]M.-T. Cheng, S.-D. Liu, H.-J. Zhou, Z.-H. Hao, and Q.-Q. Wang, Opt. Lett. **32**, 2125 (2007).
[3]J.-Y. Yan, W. Zhang, S.-Q. Duan, X.-G. Zhao, and A. O. Govorov, Phys. Rev. B **77**, 165301 (2008).
[4]R. D. Artuso and G. W. Bryant, Nano Lett. **8**, 2106 (2008).
[5]Z. Lu and K.-D. Zhu, J. Phys. B **41**, 185503 (2008).
[6]S. M. Sadeghi, Nanotechnology **20**, 225401 (2009); Phys. Rev. B **79**, 233309 (2009).
[7]Z. Lu and K.-D. Zhu, J. Phys. B **42**, 015502 (2009).
[8]S. M. Sadeghi, L. Deng, X. Li, and W.-P. Huang, Nanotechnology **20**, 365401 (2009).
[9]S. M. Sadeghi, Nanotechnology **21**, 355501 (2010); Phys. Rev. B **82**, 035413 (2010).
[10]A. Ridolfo, O. Di Stefano, N. Fina, R. Saija, and S. Savasta, Phys. Rev. Lett. **105**, 263601 (2010).
[11]E. Waks and D. Sridharan, Phys. Rev. A **82**, 043845 (2010).
[12]S. M. Sadeghi, Nanotechnology **21**, 455401 (2010).
[13]A. O. Govorov, Phys. Rev. B **82**, 155322 (2010).
[14]R. D. Artuso and G. W. Bryant, Phys. Rev. B **82**, 195419 (2010).
[15]R. D. Artuso, G. W. Bryant, A. Garcia-Etxarri, and J. Aizpurua, Phys. Rev. B **83**, 235406 (2011).
[16]A. V. Malyshev and V. A. Malyshev, Phys. Rev. B **84**, 035314 (2011).
[17]M. R. Singh, D. G. Schindel, and A. Hatef, Appl. Phys. Lett. **99**, 181106 (2011).
[18]S. M. Sadeghi and R. G. West, J. Phys.: Condens. Matter **23**, 425302 (2011).
[19]J.-B. Li, N.-C. Kim, M.-T. Cheng, L. Zhou, Z.-H. Hao, and Q.-Q. Wang, Opt. Express **20**, 1856 (2012).
[20]A. Hatef, S. M. Sadeghi, and M. R. Singh, Nanotechnology **23**, 205203 (2012).
[21]M. A. Antón, F. Carreño, S. Melle, O. G. Calderón, E. Cabrera-Granado, J. Cox, and M. R. Singh, Phys. Rev. B **86**, 155305 (2012).
[22]S. G. Kosionis, A. F. Terzis, V. Yannopapas, and E. Paspalakis, J. Phys. Chem. C **116**, 23663 (2012).
[23]S. M. Sadeghi, Appl. Phys. Lett. **101**, 213102 (2012).
[24]S. G. Kosionis, A. F. Terzis, S. M. Sadeghi, and E. Paspalakis, J. Phys.: Condens. Matter **25**, 045304 (2013).
[25]A. Hatef, S. M. Sadeghi, E. Boulais, and M. Meunier, Nanotechnology **24**, 015502 (2013).
[26]A. Hatef, S. M. Sadeghi, S. Fortin-Deschenes, E. Boulais, and M. Meunier, Opt. Express **21**, 5643 (2013).
[27]M. R. Singh, Nanotechnology **24**, 125701 (2013).

[28]M. A. Antón, F. Carreño, S. Melle, O. G. Calderón, E. Cabrera-Granado, and M. R. Singh, Phys. Rev. B **87**, 195303 (2013).
[29]E. Paspalakis, S. Evangelou, and A. F. Terzis, Phys. Rev. B **87**, 235302 (2013).
[30]B. S. Nugroho, A. A. Iskandar, V. A. Malyshev, and J. Knoester, J. Chem. Phys. **139**, 014303 (2013).
[31]M. E. Tasgin, Nanoscale **5**, 8616 (2013).
[32]S. M. Sadeghi, Phys. Rev. A **88**, 013831 (2013).
[33]S. M. Sadeghi, A. Hatef, S. Fortin-Deschenes, and M. Meunier, Nanotechnology **24**, 205201 (2013).
[34]X. N. Liu, D. Z. Yao, H. M. Zhou, F. Chen, and G. G. Xiong, Appl. Phys. B **113**, 603 (2013).
[35]S. M. Sadeghi and K. D. Patty, J. Opt. Soc. Am. B **31**, 120 (2014).
[36]P. Vasa *et al*., Phys. Rev. Lett. **101**, 116801 (2008).
[37]J.-T. Zhang, Y. Tang, K. Lee, and M. Ouyang, Nature **466**, 91 (2010).
[38]M. L. Andersen, S. Stobbe, A. S. Sorensen, and P. Lodahl, Nat. Phys. **7**, 215 (2011).
[39]N. T. Fofang, N. K. Grady, Z.-Y. Fan, A. O. Govorov, and N. J. Halas, Nano Lett. **11**, 1556 (2011).
[40]S. M. Sadeghi, R. G. West, and A. Nejat, Nanotechnology **22**, 405202 (2011); R. G. West and S. M. Sadeghi, J. Phys. Chem. C **116**, 20496 (2012).
[41]P. Vasa *et al*., Nat. Photonics **7**, 128 (2013).
[42]J. D. Cox, M. R. Singh, C. von Bilderling, and A. V. Bragas, Adv. Opt. Mater. **1**, 460 (2013).
[43]M. S. Tame, K. R. McEnery, S. K. Ozdemir, J. Lee, S. A. Maier, and M. S. Kim, Nat. Phys. **9**, 329 (2013).
[44]S. L. Sewall, A. Franceschetti, R. R. Cooney, A. Zunger, and P. Kambhampati, Phys. Rev. B **80**, 081310(R) (2009).
[45]R. W. Boyd, M. G. Raymer, P. Narum, and D. J. Harter, Phys. Rev. A **24**, 411 (1981).
[46]R. W. Boyd, *Nonlinear Optics*, 2nd ed. (Academic Press, San Diego, 2003), Chap. 6.6.
[47]H. Friedmann and A. D. Wilson-Gordon, Phys. Rev. A **57**, 4854 (1998).
[48]S. G. Kosionis, A. F. Terzis, and E. Paspalakis, Appl. Phys. B **104**, 33 (2011); J. Lumin. **140**, 130 (2013).
[49]P. B. Johnson and R. W. Christy, Phys. Rev. B **6**, 4370 (1972).